



# Power Consumption Simulation of Servo Motors Focusing on the Influence of Mechanical Vibration on Motor Efficiency

Rigacci, Massimiliano

Sato, Ryuta

Shirase, Keiichi

---

## (Citation)

International Journal of Automation Technology, 16(1):104-116

## (Issue Date)

2022-01-05

## (Resource Type)

journal article

## (Version)

Version of Record

## (Rights)

© Fuji Technology Press Ltd.

This is an Open Access article distributed under the terms of the Creative Commons Attribution-NoDerivatives 4.0 International License

(<http://creativecommons.org/licenses/by-nd/4.0/>)

## (URL)

<https://hdl.handle.net/20.500.14094/90008960>



Paper:

# Power Consumption Simulation of Servo Motors Focusing on the Influence of Mechanical Vibration on Motor Efficiency

Massimiliano Rigacci, Ryuta Sato<sup>†</sup>, and Keiichi Shirase

Department of Mechanical Engineering, Kobe University  
1-1 Rokkodai, Nada-ku, Kobe, Hyogo 657-8501, Japan

<sup>†</sup>Corresponding author, E-mail: sato@mech.kobe-u.ac.jp

[Received May 22, 2021; accepted August 3, 2021]

**This paper presents a simulation method for the power consumption of servo motors, focusing on the influence of vibrations on the motor efficiency. An apparatus consisting of two servo motors connected through a coupling was specifically designed for this study. The efficiency of the servo motor was experimentally investigated for several torque vibration levels imposed through the selection of the control parameters, and the torque vibration level was quantified through the standard deviation of the torque signal. The efficiency map characteristics for each torque oscillating level were determined. A numerical model of the apparatus clarifying the dependency of the coupling characteristics on the oscillating torque was developed, and the torque oscillation of the system was simulated. A model based on the measured motor efficiency maps and the torque oscillation level was developed to simulate the motor efficiency under several torque vibrating conditions. Finally, the power consumption of the motor was simulated based on the simulated efficiency and mechanical power. A balance of input, output, and loss powers was presented, and the experimental measurements were compared with the simulation results. The power consumption of the motor increased when the torque oscillated owing to vibrations, and the loss of power due to both oscillations and the loss of motor efficiency was quantified.**

**Keywords:** power consumption, motor efficiency, torque oscillation, coupling characteristics

## 1. Introduction

The trend of global warming, which is attributed to greenhouse gas emissions, affects the quality of life and health of human beings. Most greenhouse gases are produced by the combustion of fossil fuels. In this regard, 66% of electricity is produced by burning coal, gas, or oil [1], and 60%–80% of the electricity used in the industrial sector is consumed by electric motors [2]. Thus, improving the efficiency of electric motors can reduce greenhouse gas emissions.

The efficiency of electric motors has been investigated

by several researchers; specifically, the efficiency of permanent magnet synchronous motors (PMSMs) has been investigated in [3–6]. A discussion on the state-of-the-art loss minimization techniques to achieve a high efficiency was presented in [7]. Among these techniques, loss minimization methods based on mathematical functions of the losses were developed in [8]. Other techniques based on adaptive routines, such as the maximization of the active power through control variable adjustment, were proposed in [9]; the effects of rotor shapes and magnet skewing on vibration reduction were investigated in [10] and [11, 12], respectively. Applications, such as feed drive systems, motor efficiency, and total feed drive system power consumption, have been experimentally investigated in [13, 14]. Moreover, as in almost all industrial applications, electric motors are connected to other components through couplings (or joints), and the dynamic characteristics of the coupling should also be considered. Viscous-damping identification methods in linear vibration were investigated in [15–18], whereas theoretical characteristic identification methods were proposed in [19, 20]. Mechanical systems are commonly affected by vibrations owing to several causes, such as imbalance, misalignment, and wear [21].

The design of adequate mechanical and control systems based on sufficient knowledge is important to achieve an energy-efficient system and to perform simulations based on a model that can estimate the energy consumption. However, the effect of vibrations on motor efficiency or a simulation method of motor electric efficiency with respect to vibrations has not been investigated yet. Moreover, although some simulation methods have been proposed for the efficiency of motor drive [22] and electric powertrains [23], no explicit method for the simulation of motor electric efficiency has not been proposed yet.

Thus, this study aimed to develop a simulation method for the power consumption of electric motors, focusing on the effect of torque oscillations on motor efficiency and power consumption. Therefore, an experimental apparatus designed to measure motor efficiency and an efficiency calculation method are presented. Identification methods for the characteristics of the coupling are then presented, and torque oscillations are simulated. Finally, the effect of torque oscillations on the motor efficiency is described, and a method for simulating power consumption is pre-

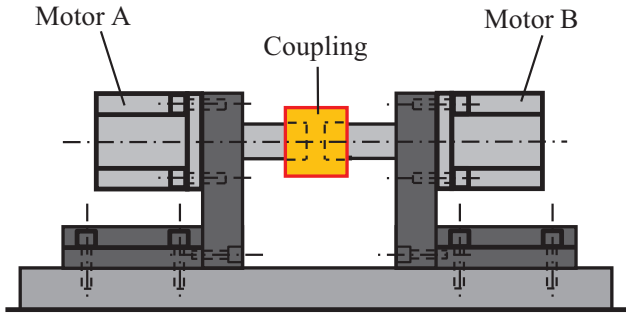


Fig. 1. Experimental apparatus.

Table 1. Specifications of motor and ball-screw.

Rated velocity	1500 rpm
Rated torque	2.86 Nm
Rated power	450 W

sented and discussed. The results indicate that the motor efficiency decreases when vibration occurs.

## 2. Experimental Apparatus and Measurement Method

### 2.1. Apparatus Description

The apparatus used in this study is shown in Fig. 1. It consists of two servo motors: A (left side) and B (right side). Both are three-phase PMSMs (Yaskawa SGMGV-05ADA21), with the rated values listed in Table 1. The two motors face each other and are connected through a coupling. Fig. 2 shows the leaf-spring coupling used in this study, which consists of an aluminum hub and four steel leaf springs.

Both motor drivers were used as the torque control mode, and the torque command signals for both motors were applied from a personal computer (PC) with a digital signal processor (DSP) board (dSPACE DS1104). The torque command for motor B was necessary to impose a load torque on motor A. The rotational angles of both motors were acquired using the DSP board at a frequency of 4000 Hz. The rotational velocity of the motors was obtained from the acquired rotational angle.

Figure 3 shows the proportional-integral (PI) velocity control system of motor A, where  $K_{vp}$  and  $K_{vi}$  are the proportional and integral gains, respectively,  $\dot{\theta}_{ref}$  and  $\dot{\theta}_m$  are the command and feedback velocities, respectively, and  $T_{ref}$  is the torque command for the servo driver.

### 2.2. Measurement Method for Mechanical Power

The mechanical quantities considered in this analysis were calculated using Eq. (1). These quantities were obtained from the control system.

In this equation,  $\tau_{ave}$  and  $\omega_{ave}$  represent the average torque and angular velocity, respectively,  $\tau_{oscill}$  and  $\omega_{oscill}$

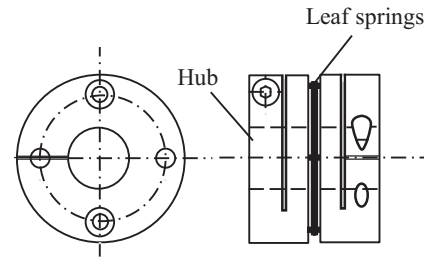


Fig. 2. Examined leaf spring coupling.

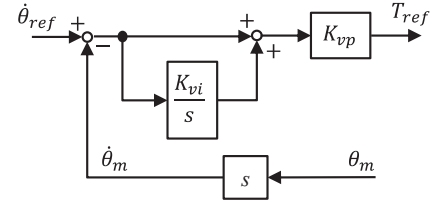


Fig. 3. Block diagram of velocity control system.

represent the oscillating components of torque and angular velocity, respectively, and  $P_{main}^m$ ,  $P_{oscill}^m$ , and  $P_{overall}^m$  represent the main, oscillating, and overall powers, respectively.

$$\left\{ \begin{array}{l} \tau_{ave} = \frac{1}{n} \sum_{k=1}^n \tau_k, \\ \omega_{ave} = \frac{1}{n} \sum_{k=1}^n \omega_k, \\ \tau_{oscill} = \frac{1}{n} \sum_{k=1}^n (\tau_k - \tau_{ave}), \\ \omega_{oscill} = \frac{1}{n} \sum_{k=1}^n (\omega_k - \omega_{ave}), \\ P_{main}^m = \tau_{ave} * \omega_{ave}, \\ P_{oscill}^m = \frac{1}{T} \int \tau_{oscill}(t) * \omega_{oscill}(t) dt, \\ P_{overall}^m = \frac{1}{T} \int \tau(t) * \omega(t) dt. \end{array} \right. \quad \dots \quad (1)$$

### 2.3. Measurement of Electric Power

The electric-quantity measurement method is shown in Fig. 4. The measured quantities were the phase current, measured with amperometric clamps, and the voltage across two phases, measured with differential probes. As the motor is a three-phase motor without a neutral wire, the electric power can be calculated using only two currents and two differential voltages, as shown in Eq. (2).

$$\left\{ \begin{array}{l} P = E_1 I_1 + E_2 I_2 + E_3 I_3 = W_a + W_b + W_c, \\ I_1 + I_2 + I_3 = 0, \\ P = E_1 I_1 + E_2 (-I_1 - I_3) + E_3 I_3, \\ P = (E_1 - E_2) I_1 + (E_3 - E_2) I_3 \\ = V_{12} I_1 + V_{32} I_3 = W_a + W_b, \end{array} \right. \quad \dots \quad (2)$$

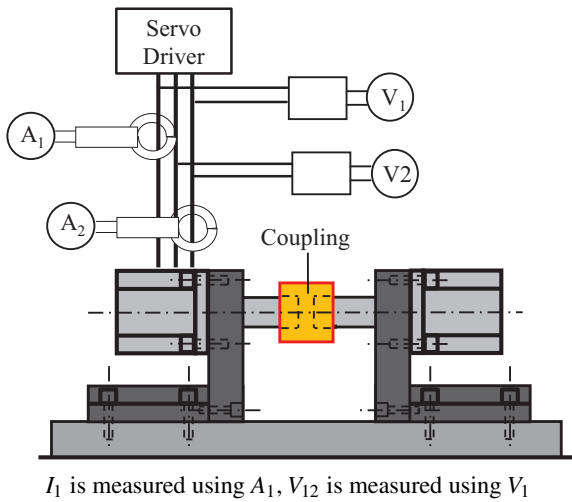


**Fig. 4.** Electric power measurement method.

where  $E_1$ ,  $E_2$ , and  $E_3$  are the voltages of each phase,  $I_1$ ,  $I_2$ , and  $I_3$  are the currents of each phase, and  $W_a$ ,  $W_b$ , and  $W_c$  are the electric powers of each phase. Each voltage and current signal was amplified and filtered using a low-pass filter with a cutoff frequency of 1600 Hz. A PC with the DSP was used for both data acquisition and motor control, and the data sampling frequency was set to 4000 Hz. After the acquisition of the signals, the apparent electric power was calculated using Eq. (3) as follows:

$$\begin{cases} V_{rms} = \sqrt{\frac{1}{n} \sum_{k=1}^n \{V_k\}^2}, \\ I_{rms} = \sqrt{\frac{1}{n} \sum_{k=1}^n \{I_k\}^2}, \\ P_{app}^e = \sum_{k=1}^2 V_{rms}^k * I_{rms}^k, \end{cases} \quad \dots \quad (3)$$

where  $V_k$  and  $I_k$  are the  $k$ -th voltage across the two phases and the current along the phase, respectively;  $V_{rms}$  and  $I_{rms}$  are the relative root mean squares of the aforementioned parameters, respectively, and  $P_{app}^e$  is the apparent electric power.

## 2.4. Measurement of Motor Efficiency

The efficiency of the motor was calculated using Eq. (4).

$$\eta_e = \frac{P_{main}^m}{P_{app}^e} = \frac{\tau_{ave} \omega_{ave}}{\sum_{k=1}^2 V_{rms}^k * I_{rms}^k} \quad \dots \quad (4)$$

The efficiency was calculated as the ratio between the only useful output of the motor – that is, the main power – and the apparent power, considered as the input. Thus, the oscillations of the output power owing to dynamic phenomena were not considered as useful outputs.

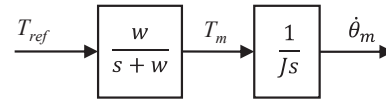


**Fig. 5.** Block diagram of a motor with an electric part.

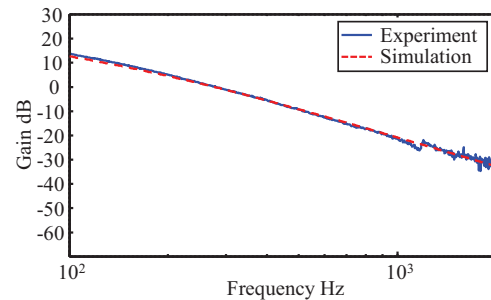


**Fig. 6.** Measured and simulated frequency characteristics of a motor.

## 3. Modeling of the Apparatus

The model of the apparatus considered in this study consisted of writing and solving the system dynamic equations to obtain the system transfer functions. Based on these functions, a block diagram was drawn and a simulation was performed to determine the coupling characteristics. The electrical and mechanical components were modeled separately.

### 3.1. Electrical Part of the Apparatus

To simplify the analysis, the electric characteristics of the servo drive, such as the motor, amplifier, and current loop, were modeled as a first-order transfer function with the cut-off angular frequency  $w$ . **Fig. 5** shows the block diagram of the electric part, including the motor. The motor was modeled as a simple rotational inertia of the moment of inertia  $J$ . The friction characteristics of the motor bearings were neglected because they did not visibly affect the obtained results. In the figure,  $T_{ref}$  and  $T_m$  are the torque command applied to the driver and the generated motor torque, respectively, and  $\dot{\theta}_m$  is the rotational velocity of the motor. The motor inertial characteristic  $J$  was determined from the specifications provided by the motor manufacturer, whereas the cut-off frequency  $w$  was required to be determined. To determine the frequency  $w$ , a logarithmic torque sweep signal with a frequency between 100 Hz and 2000 Hz was imposed on the motor through a servo analyzer (Ono Sokki DS-3000 series). The value of  $w$  that provided good agreement between the system response and the simulated one was determined to be 1200 rad/s. The measured and simulated results exhibited good agreement up to 1 kHz (**Fig. 6**).

### 3.2. Mechanical Part of the Apparatus

The two-degrees-of-freedom vibration model of the apparatus is shown in **Fig. 7**. The model considered the moment of inertia of motors A and B,  $J_a$  and  $J_b$ , respectively,

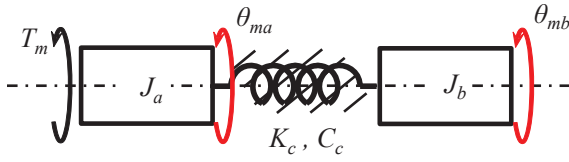


Fig. 7. Vibration model of the apparatus.

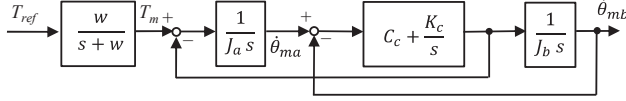


Fig. 8. Block diagram of the experimental apparatus.

the angular velocity of the motors,  $\dot{\theta}_{ma}$  and  $\dot{\theta}_{mb}$ , respectively, and the coupling stiffness and damping characteristics,  $K_c$  and  $C_c$ , respectively. The inertia of the coupling was not explicitly considered; however, it was divided into two parts, where half the inertia was attributed to motor A and half to motor B. Therefore, in this study, the stiffness  $K_c$  and damping  $C_c$  of the coupling included both the coupling and motor shaft characteristics. Thus, the equation of motion when an external torque  $T_m$  is applied can be expressed as follows:

$$\begin{cases} J_a \ddot{\theta}_{ma} + C_c (\dot{\theta}_{ma} - \dot{\theta}_{mb}) + K_c (\theta_{ma} - \theta_{mb}) = T_m, \\ J_b \ddot{\theta}_{mb} + C_c (\dot{\theta}_{mb} - \dot{\theta}_{ma}) + K_c (\theta_{mb} - \theta_{ma}) = 0. \end{cases} \quad (5)$$

Solving Eq. (5), the block diagram shown in Fig. 8 was obtained.

The friction characteristics of motors affect their energy consumption [13]. However, as investigations indicate that the influence of the friction torque of the motor is not significant compared with the vibration characteristics, friction torques were not considered in the model.

The frequency response of the apparatus was influenced by both the electric part of the motor and the coupling characteristics, as described above. The identification method for coupling characteristics determined the coupling stiffness first from the measured resonance frequency and then determined the coupling damping from the system response magnitude at the resonance frequency.

As shown in Fig. 6, the response of the electric part of the apparatus affected the magnitude of the apparatus response, but not the resonance frequency. Thus, the coupling stiffness can be determined based only on the measured resonance frequency. Therefore, starting from Eq. (4) and considering the undamped system, the equations are written as follows:

$$\begin{cases} J_a \ddot{\theta}_{ma} + K_c (\theta_{ma} - \theta_{mb}) = T_m, \\ J_b \ddot{\theta}_{mb} + K_c (\theta_{mb} - \theta_{ma}) = 0. \end{cases} \quad (6)$$

Considering sinusoidal solutions as

$$\begin{cases} \theta_{ma} = \theta_{ma} \sin \omega t, \\ \theta_{mb} = \theta_{mb} \sin \omega t. \end{cases} \quad (7)$$

Substituting Eq. (7) into Eq. (6) yields

$$\begin{cases} -\omega^2 J_a \theta_{ma} + K_c (\theta_{ma} - \theta_{mb}) = T_m, \\ -\omega^2 J_b \theta_{mb} + K_c (\theta_{mb} - \theta_{ma}) = 0. \end{cases} \quad (8)$$

Solving Eq. (8) with respect to  $\theta_{ma}$  yields the following transfer function:

$$\frac{\theta_{ma}}{T_m} = \frac{1}{\omega^2 (\omega^2 J_a J_b - K_c (J_a + J_b))}. \quad (9)$$

Considering the nontrivial solutions of the denominator, the resonance angular frequency  $\omega_0$  is formulated as

$$\omega_0 = \sqrt{\frac{K_c (J_a + J_b)}{J_a J_b}}. \quad (10)$$

Hence, the coupling stiffness can be written as

$$K_c = \frac{J_a J_b (2\pi f_0)^2}{J_a + J_b}, \quad (11)$$

where  $f_0$  is the measured resonance frequency.

As stated above, the damping coefficient identification was based on the magnification of the system response at the resonance frequency. Thus, from Eq. (5), the transfer functions between the angular velocities  $\dot{\theta}_{ma}$  or  $\dot{\theta}_{mb}$  and the motor torque  $T_m$  are expressed as follows:

$$\begin{cases} G_A(s) = \frac{\dot{\theta}_{ma}}{T_m} = \frac{J_b s^2 + C_c s + K_c}{J_a J_b s^3 + (J_a + J_b) C_c s^2 + (J_a + J_b) K_c s}, \\ G_B(s) = \frac{\dot{\theta}_{mb}}{T_m} = \frac{C_c s + K_c}{J_a J_b s^3 + (J_a + J_b) C_c s^2 + (J_a + J_b) K_c s}, \end{cases} \quad (12)$$

where  $G_A(s)$  and  $G_B(s)$  are the transfer functions for motors A and B, respectively.

The magnitudes of the resonance frequencies can be obtained from the transfer functions in Eq. (12), as shown in Eq. (13), where  $M_{Af0}$  and  $M_{Bf0}$  represent the response magnifications of  $\dot{\theta}_{ma}$  and  $\dot{\theta}_{mb}$ , respectively.

$$\begin{cases} M_{Af0} = \frac{\sqrt{\frac{(J_a + J_b)^4}{J_a^4} K_c^4 C_c^2 + \frac{(J_a + J_b)^5}{J_a^3 J_b^3} K_c^3 C_c^4}}{\frac{(J_a + J_b)^4}{J_a^2 J_b^2} K_c^2 C_c^2}, \\ M_{Bf0} = \frac{\sqrt{\frac{(J_a + J_b)^4}{J_a^2 J_b^2} K_c^4 C_c^2 + \frac{(J_a + J_b)^5}{J_a^3 J_b^3} K_c^3 C_c^4}}{\frac{(J_a + J_b)^4}{J_a^2 J_b^2} K_c^2 C_c^2}. \end{cases} \quad (13)$$

The above equations involve only the mechanical system; however, the measured system frequency response is affected by the electrical part, with the cut-off frequency  $w$ ; thus, considering the response magnification,



owing to the electrical part at the resonance frequency, Eq. (14) can be obtained as

$$M_{f0w} = \frac{w}{\sqrt{\frac{K_c(J_a + J_b)}{J_a J_b} + (w)^2}}, \quad \dots \quad (14)$$

where  $M_{f0w}$  is the magnification of the electrical part with the determined cut-off frequency  $w$ . Thus, the final magnitude of the magnification of  $\dot{\theta}_{ma}$  and  $\dot{\theta}_{mb}$  is the product of the magnifications owing to the electrical part and the mechanical system, as follows:

$$\left\{ \begin{array}{l} M_{Af}^{exp} = \frac{w}{\sqrt{\frac{K_c(J_a + J_b)}{J_a J_b} + (w)^2}} M_{Af0} \\ \quad \equiv M_{f0w} M_{Af0}, \\ M_{Bf}^{exp} = \frac{1}{T_f} \frac{1}{\sqrt{\frac{K_c(J_a + J_b)}{J_a J_b} + \left(\frac{1}{T_f}\right)^2}} M_{Bf0} \\ \quad \equiv M_{f0w} M_{Bf0}. \end{array} \right. \quad (15)$$

The damping coefficient can be expressed using Eqs. (13)–(15) as follows:

$$\left\{ \begin{array}{l} C_c = \sqrt{\frac{K_c J_b^4}{K_c(J_a + J_b)^4 \left(\frac{M_{Af}^{exp}}{M_{f0w}}\right)^2 - J_a J_b(J_a + J_b)}}, \\ C_c = \sqrt{\frac{K_c J_a^2 J_b^2}{K_c(J_a + J_b)^4 \left(\frac{M_{Bf}^{exp}}{M_{f0w}}\right)^2 - J_a J_b(J_a + J_b)}}, \end{array} \right. \quad \dots \quad (16)$$

where  $M_{Af}^{exp}$  and  $M_{Bf}^{exp}$  are the measured magnifications at the resonance frequencies for motors A and B, respectively. In this study, the apparatus consisted of two identical motors; thus,  $J_a$  and  $J_b$  were equal. Moreover, it was assumed that  $M_{Af}^{exp} = M_{Bf}^{exp} = M_f^{exp}$ . Thus, the damping coefficient becomes

$$C_c = \sqrt{\frac{K_c J_a}{16 K_c J_a \left(\frac{M_f^{exp}}{M_{f0w}}\right)^2 - 2}} \quad \dots \quad (17)$$

Similar to the determination of the cut-off frequency for the electric part, to determine the coupling stiffness and damping, a sweep signal with frequencies between 100 Hz and 2000 Hz was imposed on motor A through a servo analyzer. The coupling stiffness is determined using Eq. (11), whereas the coupling damping is determined using Eq. (17). An example of the measured and simulated apparatus frequency responses is presented in Fig. 9. The response of both motors showed a resonance frequency of approximately 850 Hz, whereas motor B showed an antiresonance frequency of approximately 600 Hz. Considering a torque sweep magnitude of 1.5 Nm, the coupling stiffness was determined to be 4978 Nm/rad and the

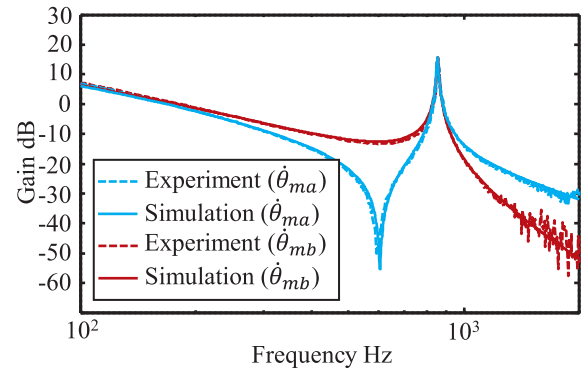


Fig. 9. Example of measured and simulated frequency characteristics.

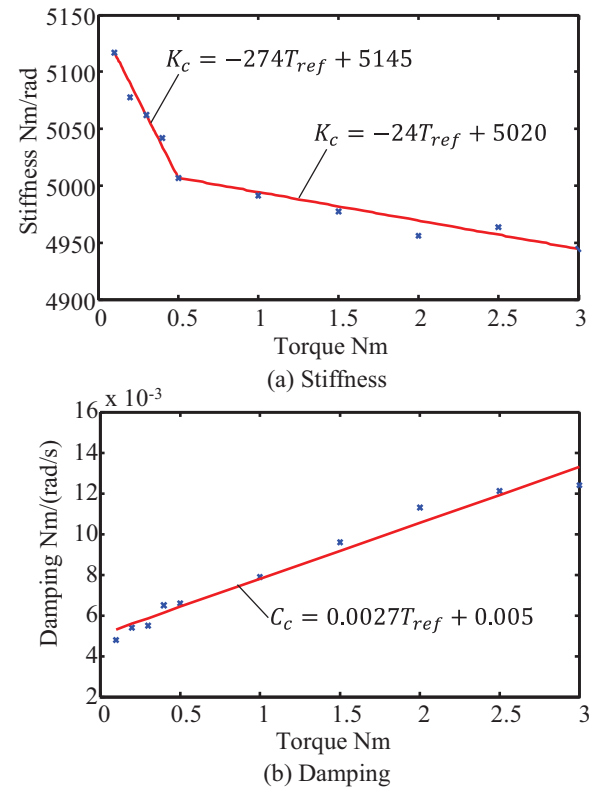
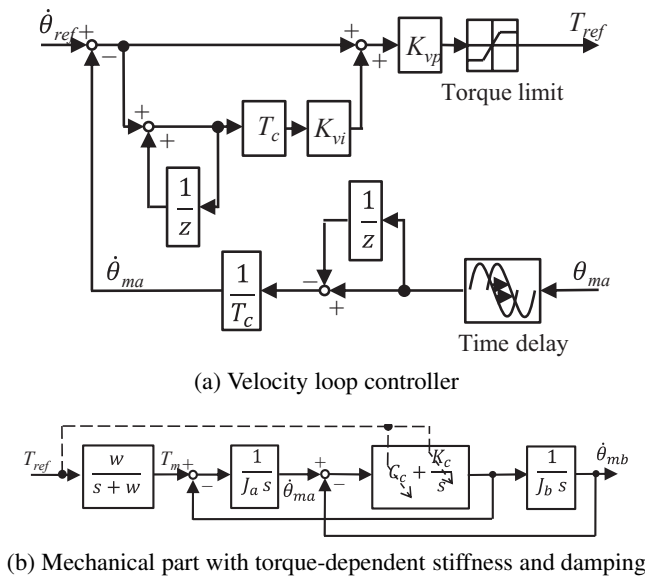


Fig. 10. Approximation of torque dependent stiffness and damping for the simulation.

damping was determined to be 0.094 Nm/(rad/s).

The coupling characteristics were determined for the torque magnitude of the input frequency sweep between 0.1 Nm and 3 Nm. Fig. 10 shows the relationship between the coupling characteristics and the sweep torque, and the analytical equations. The results showed that the stiffness and damping of the coupling were related to the motor torque [24]. The nonlinear characteristics of the leaf springs of the coupling and the contact between the clump hub of the coupling and the motor shaft were expected to affect the torque dependency of the coupling characteristics. The reason for the change in the characteristics will be investigated in the next part of the study.



**Fig. 11.** Block diagram with torque dependent characteristics for velocity step response simulation.

### 3.3. Velocity Control System and Torque-Dependent Coupling Model

**Figure 11** shows a block diagram of the apparatus. **Fig. 11(a)** shows the block diagram of the time discrete PI velocity control loop, where  $K_{vp}$  is the proportional gain,  $K_{vi}$  is the integral gain,  $T_c$  is the control period (0.25 ms), and the block “time delay” represents the encoder signal delay, which is one control cycle. **Fig. 11(b)** shows the block diagram of the mechanical part of the apparatus, as described in Section 3.2, with torque-dependent coupling stiffness and damping. The torque-dependent characteristics were modeled as the torque command ( $T_{ref}$ ) dependent stiffness and damping based on the evaluated results shown in **Fig. 10**.

## 4. Efficiency Maps with Respect to Torque Oscillations

### 4.1. Efficiency Map Tests

A total of 360 test conditions were investigated to evaluate the motor efficiency. Each test was conducted in accordance with the following procedure: a constant load torque was applied through motor B, whereas a set of angular velocities was commanded through motor A. The set of velocities consisted of 24 angular velocities between 1 rad/s and 65 rad/s (approximately 9 rpm and 620 rpm, respectively). Initially, a constant load torque of 0.05 Nm was imposed, and the set of velocities was commanded; then, the load torque was increased in magnitude and the set of velocities was commanded again. In total, 15 load torques between 0.05 Nm and 3 Nm were imposed. For each velocity, clockwise and counter-clockwise rotating directions were considered, and pos-

itive and negative load torques were considered as well. For each test, the signals were acquired for 0.5 s during the constant-velocity motion, and only the case in which the load torque opposed the relative velocity was considered. A more detailed description of the test conditions was reported in [13].

### 4.2. Torque Oscillations

According to feedback control theory, a higher feedback gain setting yields a vibrated system. In this study, the velocity proportional gain  $K_{vp}$  was set higher to create vibrating conditions to investigate the influence of the vibration on the motor efficiency. **Fig. 12** shows the motor torque when a constant velocity of 10 rad/s was imposed on motor A for four  $K_{vp}$  values. From the figures, the torque oscillated in the case of higher  $K_{vp}$  settings. The standard deviation defined in Eq. (18) was considered to quantify the magnitude of the torque oscillation.

$$\sigma = \sqrt{\frac{1}{N} \sum_{i=1}^N (x_i - \mu)^2}, \dots \dots \dots (18)$$

where  $\sigma$  is the standard deviation,  $x_i$  is the torque value considered,  $\mu$  is the average torque in the interval, and  $N$  is the interval number of points. From the figure, the magnitude of the oscillations of torque increased for higher  $K_{vp}$  values.

**Figure 13** shows the magnitude of torque oscillation for  $K_{vp} = 0.30$ , and several angular velocities of the motor. For all the three investigated conditions, the standard deviation values were similar and close to 1.50. **Fig. 14** shows the oscillations of torque setting for a  $K_{vp}$  of 0.30 and a velocity of 10 rad/s, with several loading torques applied by motor B. The torque oscillation level is similar to that shown in **Fig. 13**. Finally, **Fig. 15** shows the torque oscillation setting for a  $K_{vp}$  of 0.30 and a velocity of 50 rad/s, with several load torques, which were similar to the previously investigated cases.

Thus, the torque oscillation level was determined by the  $K_{vp}$  setting and was not significantly affected by the working conditions of the motor.

**Figure 16(a)** shows the motor efficiency map for  $K_{vp} = 0.05$ , which represents the case where the torque signal shape is not significantly affected by vibrations. The efficiency of the motor was high for a high angular velocity and intermediate torque, whereas it was low for a very low angular velocity and high torque. When the angular velocity was set, the efficiency decreased for high torques because the copper losses were higher [25]. Indeed, the copper losses depended on the current, which depended on the motor torque.

### 4.3. Motor Efficiency with Torque Oscillations

**Figures 16(b) and (c)** show the efficiency maps for  $K_{vp} = 0.15$  and 0.30, respectively. The torque oscillations, shown in **Fig. 12**, affected the efficiency of the motor, particularly at low velocities. As evident from **Figs. 13–15**, the oscillation level was not significantly affected by the

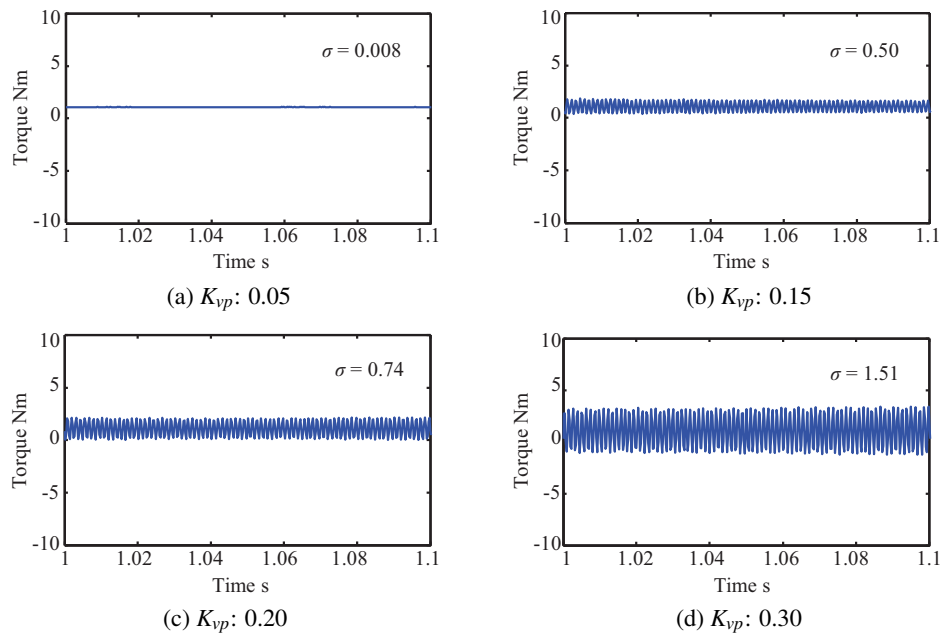


**Fig. 12.** Measured torque during the motion with different  $K_{vp}$ s.

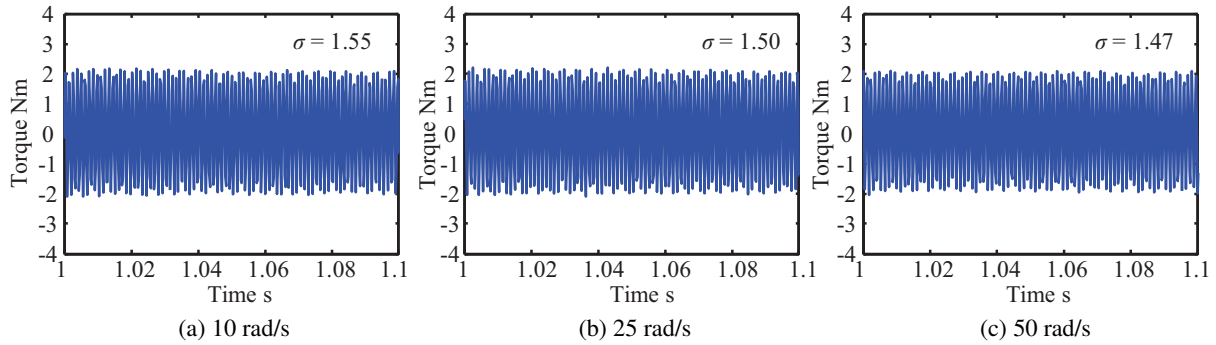


**Fig. 13.** Torque oscillation for several motor velocities (without load,  $K_{vp}$ : 0.30).

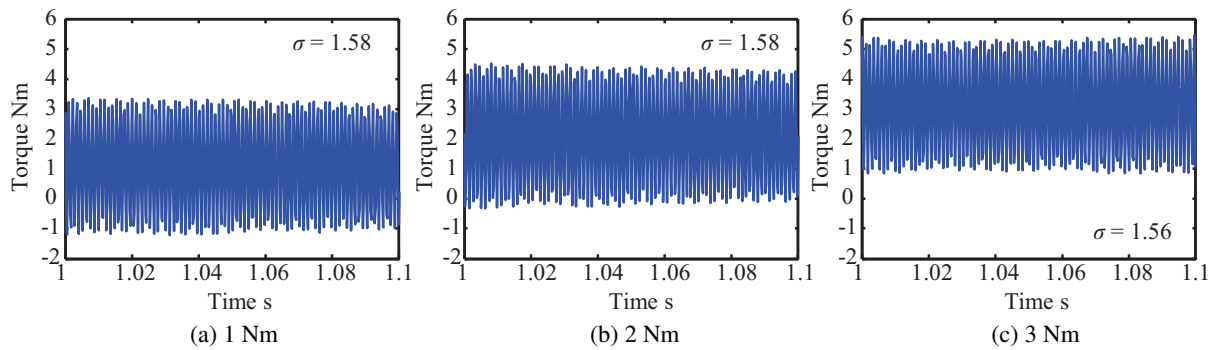


**Fig. 14.** Torque oscillation for several load torques (10 rad/s,  $K_{vp}$ : 0.30).

angular velocity or torque, but was only affected by  $K_{vp}$ . The efficiency shown in **Figs. 16(b)** and **(c)** decreased because the motor had to expend additional energy to limit the torque oscillations. For a low motor velocity, the power output was very small compared with the input power; thus, the additional power expended to limit the torque oscillation significantly affected the efficiency

of the motor. For a high motor velocity, the power output was considerably higher than the power required to suppress the torque oscillations; therefore, the decrease in efficiency was less significant, and the effect of oscillation on the motor efficiency was more severe at a low velocity. Further details about the effect of torque oscillation on motor efficiency can be found in [26]. As stated in Sec-



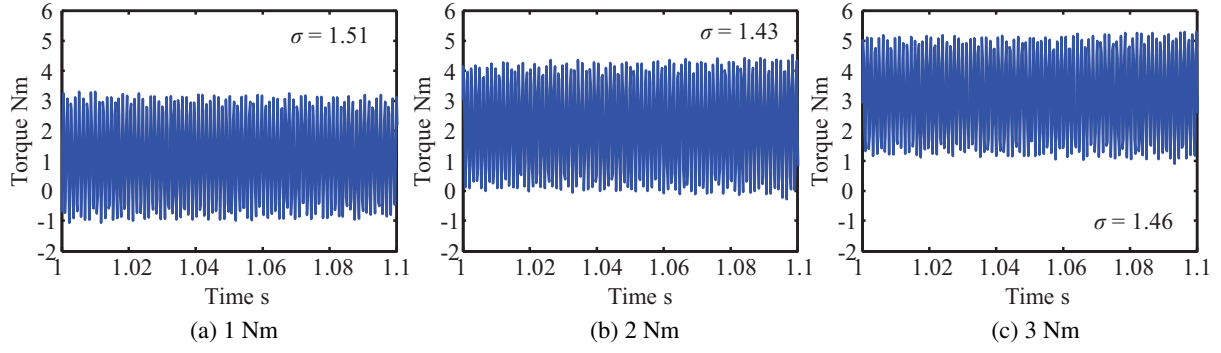


**Fig. 15.** Torque oscillation for several load torques (50 rad/s,  $K_{vp}$ : 0.30).

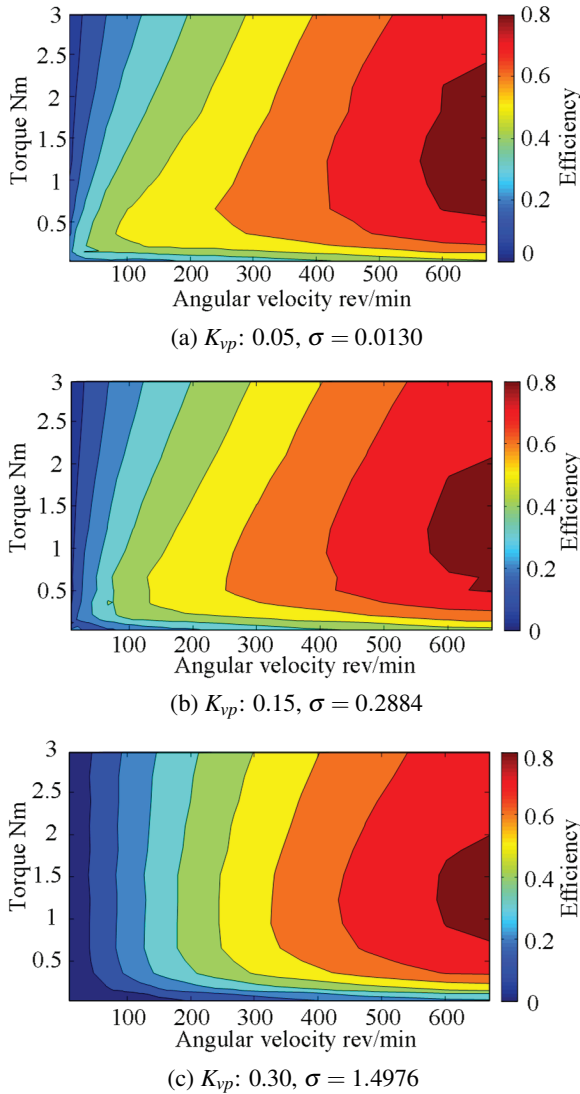


**Fig. 16.** Comparison of evaluated efficiency maps with different  $K_{vp}$ s.

tion 4.2, the torque vibration level depends exclusively on  $K_{vp}$ ; thus, the effect of torque vibrations on the motor efficiency is exclusively a function of  $K_{vp}$ . The torque standard deviation determines the torque vibration level; therefore, it determines the efficiency map.

## 5. Power Consumption Simulation

### 5.1. Simulation of Torque

In this study, the motor efficiency was modeled as a function of the velocity, torque, and torque vibration level. Therefore, vibration should be accurately simulated. **Figs. 17** and **18** show a comparison between the experimental and simulated torques for several  $K_{vp}$  values and velocities, and the load torques of 1 Nm and 3 Nm, respectively. It is apparent that the proposed model can represent the torque oscillations under all the conditions investigated.

### 5.2. Motor Efficiency Estimation

This study aimed to simulate motor electric power. **Fig. 19** shows the proposed electric power simulation method. First, the motor angular velocity and torque were simulated, and the standard deviation of the torque was used as a reference to select the efficiency map. As only three efficiency maps were determined in this study, the characteristics of the efficiency maps of three vibration levels were determined. For values of standard deviation of torque different from the known ones, the closest known values of standard deviation were taken and the linear interpolation between the two efficiency maps corresponding to the closed value of standard deviation was performed. For example, by denoting the standard deviations associated with two known efficiency maps as  $\sigma_1$  and  $\sigma_2$  and the standard deviation from the simulated torque as  $\sigma_x$ , with  $\sigma_1 < \sigma_x < \sigma_2$ , Eq. (19) expresses the identification method.

$$Eff(\sigma_x) = Eff(\sigma_1) + \frac{\sigma_x - \sigma_1}{\sigma_2 - \sigma_1} (Eff(\sigma_2) - Eff(\sigma_1)), \quad (19)$$

where  $Eff(\sigma_x)$  is the efficiency map associated with the standard deviation  $\sigma_x$ . Once the efficiency map was determined, the simulated torque and angular velocity were used to determine the motor efficiency characteristics for the specific working conditions. Finally, the electric power was simulated as the ratio of mechanical power to motor efficiency. **Fig. 20** shows the comparison between the simulated efficiency and the efficiency calculated from the experiments for several velocities and a load torque

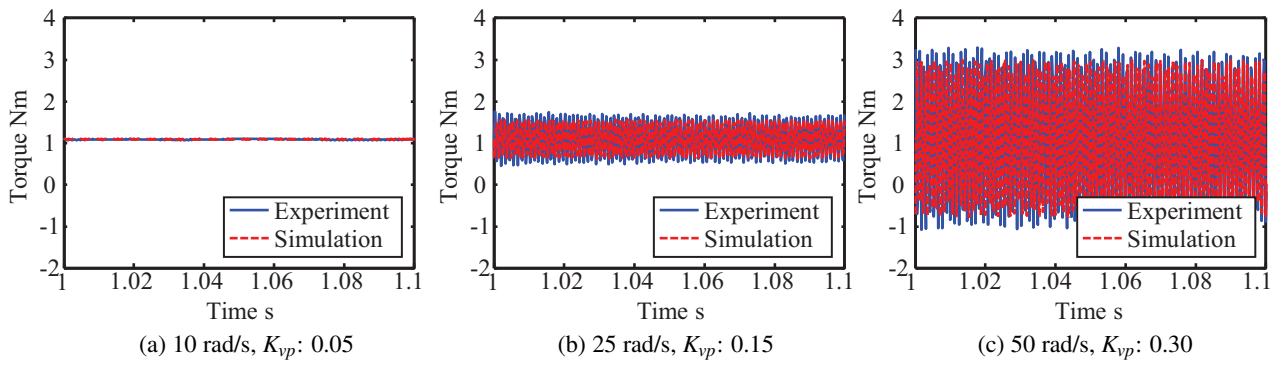


**Fig. 17.** Measured and simulated torque oscillations for several motor velocities and gains (1 Nm load).

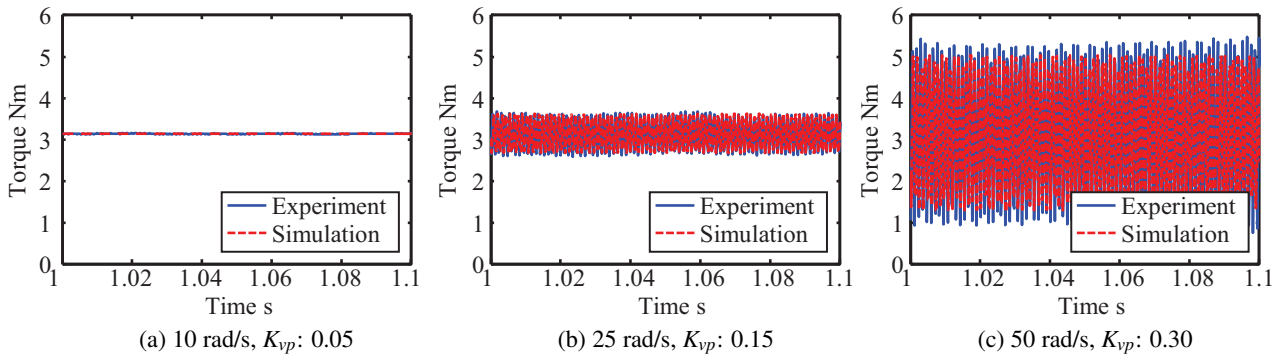


**Fig. 18.** Measured and simulated torque oscillations for several motor velocities and gains (3 Nm load).

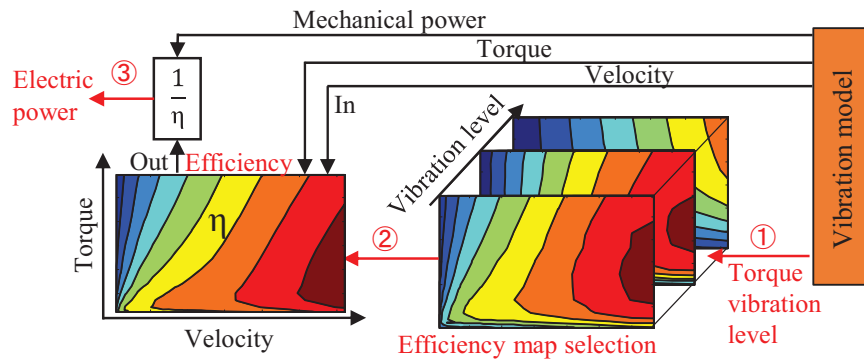


**Fig. 19.** Proposed simulation method for electric power consumption.

of 1 Nm. The lines in the figure represent the linear interpolation of the discrete values indicated by the plots. As already clarified from the efficiency map analysis, the efficiency decreased when the vibration level increased. The proposed efficiency simulation method can predict the motor efficiency with a good accuracy, particularly for the higher load torque case (see **Fig. 21**). Furthermore, the maximum error of the prediction shown in **Fig. 20(c)** is 2.6%, which indicates that the accuracy of the prediction is sufficient. However, the prediction accuracy becomes higher in the case of a higher loading torque. Although it is expected that the prediction accuracy would be affected by the signal-to-noise ratio, the reason for the differences has not been clarified.

### 5.3. Power Consumption Analysis

**Figure 22** shows the analysis of the power consumption of the motor depending on the torque vibration level for a velocity of 10 rad/s and a load torque of 1 Nm. **Fig. 22(a)** shows the power consumed to drive motor A against the imposed load torque from motor B. According to the definition given in Eq. (1), the main power was calculated from the average quantities; thus, it was not affected by vibrations and was constant. The measured and simulated results are consistent with each other. **Fig. 22(b)** shows the power consumed to suppress oscillations. As defined in Eq. (1), the power increased with the vibration level. The power was negative because the motor control applied a torque to limit the velocity oscillations; therefore, the motor torque and motor angular velocity were out of

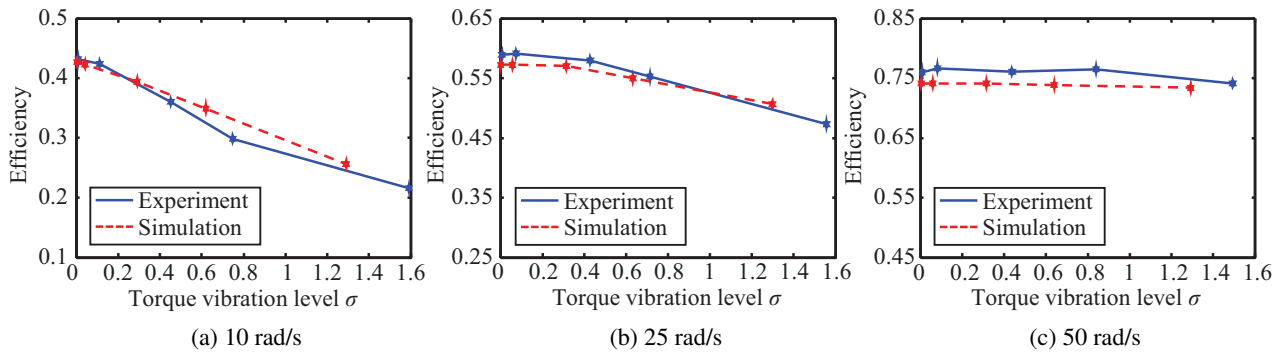


**Fig. 20.** Measured and simulated efficiency for several vibrating conditions (1 Nm load).

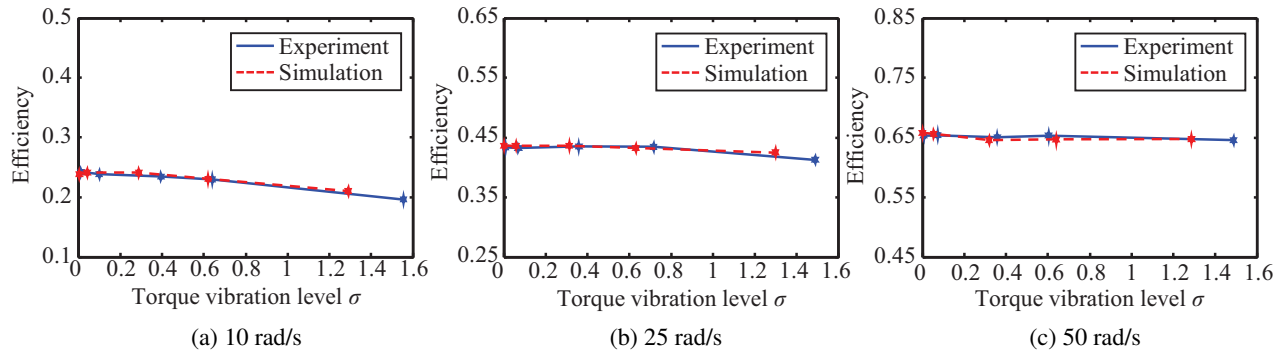


**Fig. 21.** Measured and simulated efficiencies for several vibrating conditions (3 Nm load).

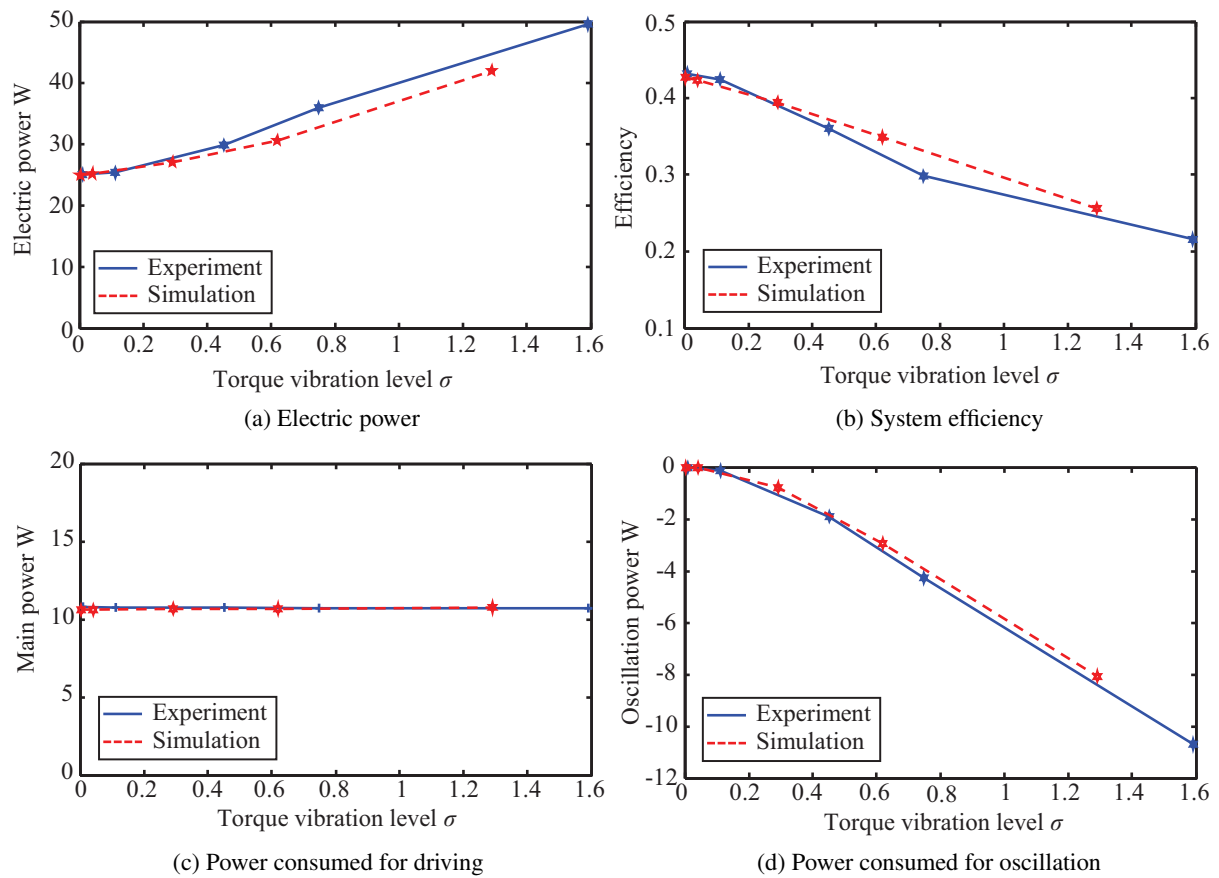


**Fig. 22.** Measured and simulated efficiencies and power balance (10 rad/s and 1 Nm load case).

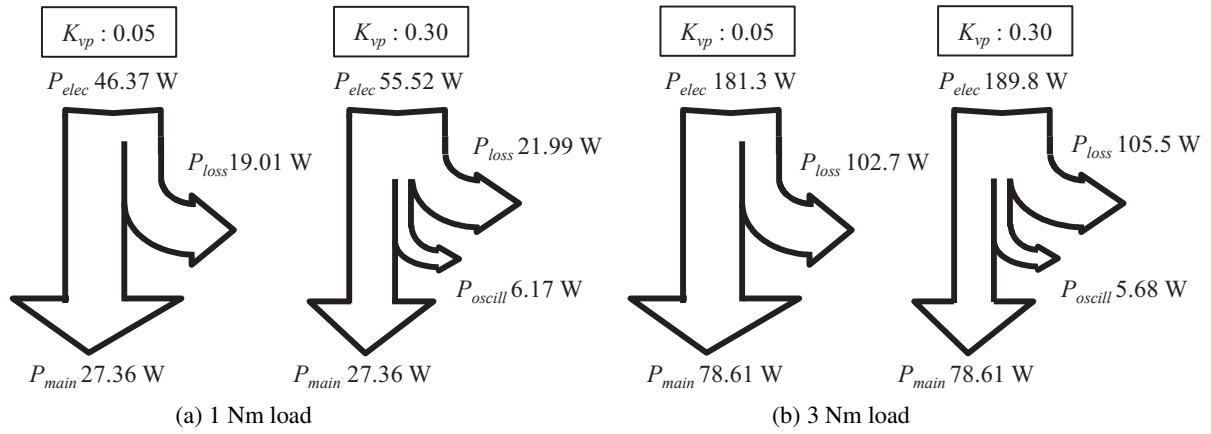


Fig. 23. Analyzed power balance based on measured results, velocity 25 rad/s.

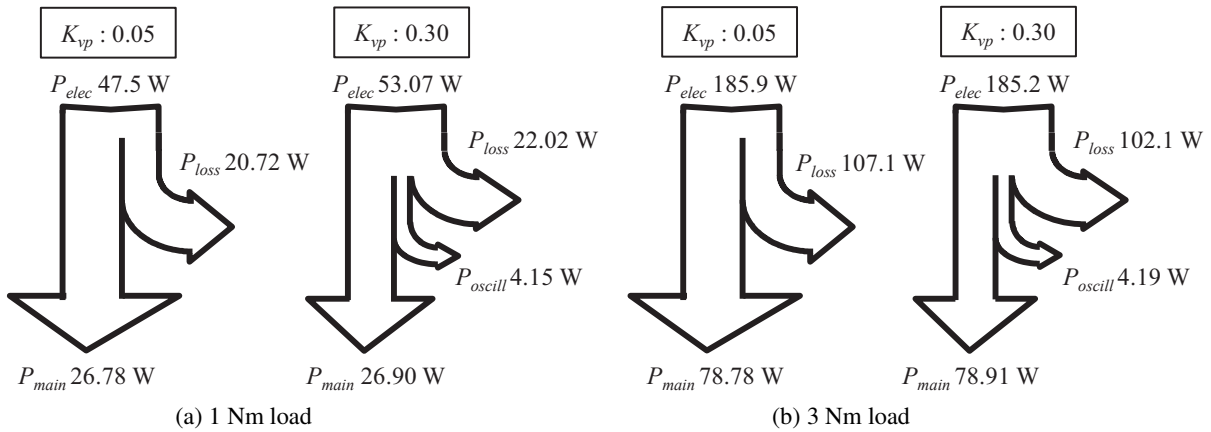


Fig. 24. Analyzed power balance based on simulated results, velocity 25 rad/s.

phase. The power of oscillation was not considered a useful output; therefore, it was not considered in the numerator of the efficiency ratio (see Eq. (4)); nevertheless, as this power was supplied by the motor, the electric power consumption increased.

Figure 22(c) shows the electric power consumption of the motor. Both the simulation and experimental results showed a positive tendency with respect to the torque vibration level, and they were consistent with each other. Fig. 22(d) shows the measured and estimated motor efficiencies. Although the simulated vibration levels were lower than the actual levels, the figures indicate that the proposed simulation method can adequately predict the power consumption depending on the torque vibration level.

Figure 23 shows an analysis of the measured motor power consumption. In case (a), comparing the motor power consumption, although the main power  $P_{main}$  and the loss power  $P_{loss}$  were the same in both cases, the electric power consumption increased in the case of  $K_{vp} = 0.30$ . This was due to the additional power supplied by the motor to limit the oscillation  $P_{oscill}$ , which did not contribute to the main power. The loss power  $P_{loss}$  is a result of the copper and iron losses, and the additional power can be estimated from the vibration level [26]. In the analy-

sis, the main power  $P_{main}$  and the additional power  $P_{oscill}$  were estimated from the measured and simulated results, and the loss power  $P_{loss}$  was assumed to be the remaining part of the power. In other words, the evaluated motor efficiency shown in Fig. 16 included the influence of both  $P_{loss}$  and  $P_{oscill}$ , and the additional power  $P_{oscill}$  increased with increasing vibration levels. The additional part of the power due to vibration can be estimated from the evaluated vibration level.

The electric power consumption increased when a higher load torque was applied, similar to the main power. In both load cases, the amount of power necessary to suppress the oscillations was similar. Fig. 24 shows the power analysis from the simulated results; the simulated powers are similar to the measured ones. Thus, the proposed method can correctly simulate the power consumption of the motor, which is influenced by vibrations. In addition, higher gain settings that oscillate the system yield energy waste. The proposed simulation method can predict the wasted energy, and it can be an effective tool for achieving a higher energy efficiency of the system by designing a proper controller and operating conditions.

## 6. Conclusions

In this paper, a method for simulating motor power consumption with respect to torque vibrations was proposed. A dedicated apparatus was built to determine the coupling dynamic characteristics and measure the motor efficiency under several vibrating conditions. The proposed simulation method considers the torque-dependent characteristics of the coupling device and motor efficiency. The following conclusions were drawn.

- 1) The motor efficiency was strongly dependent on the torque vibration level; the efficiency decreased in the high vibration case, particularly for a low motor velocity.
- 2) The electric power consumption of the motor increased under high vibrating torque conditions, as the motor expended additional power to suppress the vibrations.
- 3) The proposed model can reproduce the motor torque and efficiency with respect to torque oscillations.

In this study, a simulation method for motor electric power consumption under vibrating conditions was successfully developed. The proposed simulation method can predict the wasted energy, and it can be an effective tool for achieving a higher energy efficiency of the system by designing a proper controller and operating conditions. Moreover, through the proposed simulation method, minimum motor energy consumption can be among the system design criteria. In the future, the authors will attempt to extend the proposed method to simulate the power consumption of feed drive systems under vibrating conditions.

## References:

- [1] "World Energy Balances," 2020 Edition, Int. Energy Agency, 2020.
- [2] A. de Almeida, P. Bertoldi, and W. Leonhard, "Energy efficiency improvements in electric motors and drives," Springer, 1997.
- [3] D.-J. Sim, D.-H. Cho, J.-S. Chun, H.-K. Jung, and T.-K. Chung, "Efficiency optimization of interior permanent magnet synchronous motor using genetic algorithms," *IEEE Trans. on Magnetics*, Vol.33, No.2, pp. 1880-1883, 1997.
- [4] L. Yu, Y. Zhang, and W. Huang, "Accurate and efficient torque control of an interior permanent magnet synchronous motor in electric vehicles based on hall-effect sensors," *Energies*, Vol.10, No.3, doi: 10.3390/en10030410, 2017.
- [5] P. K. Patel, R. Nagarsheth, and S. Parnerkar, "Performance comparison of permanent magnet synchronous motor and induction motor for cooling tower application," *Int. J. of Emerging Technology and Advanced Engineering*, Vol.2, No.8, pp. 167-171, 2012.
- [6] K. Kurihara and M. A. Rahman, "High-efficiency line-start interior permanent magnet synchronous motors," *IEEE Trans. on Industry Applications*, Vol.40, No.3, pp. 789-796, 2004.
- [7] C. Cavallaro, A. O. Di Tommaso, R. Miceli, A. Raciti, G. R. Galluzzo, and M. Trapanese, "Efficiency enhancement of permanent-magnet synchronous motor drives by online loss minimization approaches," *IEEE Trans. on Industrial Electronics*, Vol.52, No.4, pp. 1153-1160, 2005.
- [8] S. Morimoto, Y. Tong, Y. Takeda, and T. Hirasaka, "Loss minimization control of permanent magnet synchronous motor drives," *IEEE Trans. on Industrial Electronics*, Vol.41, No.5, pp. 511-517, 1994.
- [9] S. Vaez, V. I. John, and M. A. Rahman, "Adaptive loss minimization control of inverter-fed IPM motor drives," *Record 28th Annual IEEE Power Electronics Specialists Conf. (PESC97)*, Vol.2, pp. 861-868, 1997.
- [10] C. M. Burt, X. Piao, F. Gaudi, B. Busch, and N. F. Taufik, "Electric motor efficiency under variable frequencies and loads," *J. of Irrigation and Drainage Engineering*, Vol.134, No.2, pp. 129-136, 2008.
- [11] H. Xie, X. Wei, Y. Liu, Y. Feng, Y. Zhang, X. Yang, and K. Yang, "Research of asymmetrical bidirectional magnet skewing technique in modular multi-stage axial flux permanent magnet synchronous motor," *IEEE Trans. on Magnetics*, Vol.51, No.3, Article Sequence No.8102705, 2015.
- [12] W.-H. Kim, K.-C. Kim, S.-J. Kim, D.-W. Kang, S.-C. Go, H.-W. Lee, Y.-D. Chun, and J. Lee, "A study on the optimal rotor design of LSPM considering the starting torque and efficiency," *IEEE Trans. on Magnetics*, Vol.45, No.3, pp. 1808-1811, 2009.
- [13] M. Rigacci, R. Sato, and K. Shirase, "Experimental evaluation of mechanical and electrical power consumption of feed drive systems driven by a ball-screw," *Precision Engineering*, Vol.64, pp. 280-287, 2020.
- [14] A. Hayashi, R. Sato, R. Iwase, M. Hashimoto, and K. Shirase, "Measurement and simulation of electric power consumption of feed drive systems," *Proc. of the ASME 2013 Int. Mechanical Engineering Congress and Exposition*, Vol.2A, 2013.
- [15] A. S. Phani and J. Woodhouse, "Viscous damping identification in linear vibration," *J. of Sound and Vibration*, Vol.303, No.3-5, pp. 475-500, 2007.
- [16] S. Adhikari and J. Woodhouse, "Identification of damping: Part 1, Viscous damping," *J. of Sound and Vibration*, Vol.243, No.1, pp. 43-61, 2001.
- [17] S. Adhikari and J. Woodhouse, "Identification of damping: Part 2, Non-viscous damping," *J. of Sound and Vibration*, Vol.243, No.1, pp. 63-88, 2001.
- [18] C. Minas and D. J. Inman, "Identification of a non-proportional damping matrix from incomplete model information," *ASME J. of Vibration and Acoustics*, Vol.113, No.2, pp. 219-224, 1991.
- [19] C.-P. Fritzen, "Identification of mass, damping and stiffness matrices of mechanical systems," *J. of Vibration, Acoustics, Stress, and Reliability in Design*, Vol.108, No.1, pp. 9-16, 1986.
- [20] Y. Pan and Y. Wang, "Iterative method for exponential damping identification," *Computer-Aided Civil and Infrastructure Engineering*, Vol.30, No.3, pp. 229-243, 2015.
- [21] C. Du and L. Xie, "Modeling and control of vibration in mechanical systems," CRC Press Taylor & Francis Group, 2018.
- [22] L. Aarniovuori, "Induction motor drive energy efficiency – Simulation and analysis," Ph.D. Thesis, Lappeenranta University of Technology, 2010.
- [23] A. Sornioti, T. Holdstock, G. L. Pilone et al., "Analysis and simulation of the gearshift methodology for a novel two-speed transmission system for electric powertrains with a central motor," *Proc. of the Institution of Mechanical Engineers, Part D: J. of Automobile Engineering*, Vol.226, No.7, pp. 915-929, 2012.
- [24] M. Rigacci, R. Sato, K. Shirase, and T. Sasaki, "Evaluation of torque-dependent coupling characteristics and their influence on the system vibration characteristics," *J. of Advanced Mechanical Design, Systems, and Manufacturing*, Vol.15, No.5, JAMDSM0060, 2021.
- [25] A. Mahmoudi, W. L. Soong, G. Pellegrino, and E. Armando, "Efficiency maps of electric machines," *2015 IEEE Energy Conversion Congress and Exposition (ECCE)*, pp. 2791-2799, 2015.
- [26] M. Rigacci, R. Sato, and K. Shirase, "Evaluating the influence of mechanical system vibration characteristics on servo motor efficiency," *Precision Engineering*, Vol.72, pp. 680-689, 2021.





**Name:**  
Massimiliano Rigacci

**Affiliation:**  
Ph.D. Student, Department of Mechanical Engineering, Graduate School of Engineering, Kobe University

**Address:**  
1-1 Rokkodai, Nada-ku, Kobe, Hyogo 657-8501, Japan

**Brief Biographical History:**  
2014 Received Bachelor degree from University of Florence  
2017 Received Master degree from University of Florence  
2018- Ph.D. Student, Kobe University

**Main Works:**

- "Evaluating the influence of mechanical system vibration characteristics on servo motor efficiency," Precision Engineering, Vol.72, pp. 680-689, 2021.
- "Experimental evaluation of mechanical and electrical power consumption of feed drive systems driven by a ball-screw," Precision Engineering, Vol.64, pp. 280-287, 2020.
- "Multibody Analysis Techniques for Vibration Characteristics of a Feed Drive System," Proc. of the 8th Int. Conf. on Positioning Technology, 2018.

**Membership in Academic Societies:**  
• Japan Society for Precision Engineering (JSPE)



**Name:**  
Ryuta Sato

**Affiliation:**  
Associate Professor, Department of Mechanical Engineering, Graduate School of Engineering, Kobe University

**Address:**  
1-1 Rokkodai, Nada-ku, Kobe, Hyogo 657-8501, Japan

**Brief Biographical History:**  
2004- Research Associate, Tokyo University of Agriculture and Technology  
2008- Researcher, Mitsubishi Electric Corporation  
2010- Assistant Professor, Kobe University  
2013- Associate Professor, Kobe University

**Main Works:**

- "Analytical Time Constant Design for Jerk-Limited Acceleration Profiles to Minimize Residual Vibration After Positioning Operation in NC Machine Tools," Precision Engineering, Vol.71, pp. 47-56, 2021.
- "Active Vibration Suppression of NC Machine Tools for High Speed Contouring Motions," J. of Advanced Mechanical Design, Systems, and Manufacturing, Vol.14, No.1, JAMDSM0005, 2020.
- "Time domain coupled simulation of machine tool dynamics and cutting forces considering the influences of nonlinear friction characteristics and process damping," Precision Engineering, Vol.61, pp. 103-109, 2020.

**Membership in Academic Societies:**  
• Japan Society of Mechanical Engineers (JSME)  
• Japan Society for Precision Engineering (JSPE)  
• Society of Instrument and Control Engineers (SICE)



**Name:**  
Keiichi Shirase

**Affiliation:**  
Professor, Department of Mechanical Engineering, Graduate School of Engineering, Kobe University

**Address:**  
1-1 Rokkodai, Nada-ku, Kobe, Hyogo 657-8501, Japan

**Brief Biographical History:**  
1984- Research Associate, Kanazawa University  
1995- Associate Professor, Kanazawa University  
1996- Associate Professor, Osaka University  
2003- Professor, Kobe University

**Main Works:**

- K. Shirase and K. Nakamoto, "Simulation Technologies for the Development of an Autonomous and Intelligent Machine Tool," Int. J. Automation Technol., Vol.7, No.1, pp. 6-15, 2013.
- T. Kobayashi, T. Hirooka, A. Hakotani, R. Sato, and K. Shirase, "Tool Motion Control Referring to Voxel Information of Removal Volume Voxel Model to Achieve Autonomous Milling Operation," Int. J. Automation Technol., Vol.8, No.6, pp. 792-800, 2014.
- M. M. Isnaini, Y. Shinoki, R. Sato, and K. Shirase, "Development of CAD-CAM Interaction System to Generate a Flexible Machining Process Plan," Int. J. Automation Technol., Vol.9, No.2, pp. 104-114, 2015.
- I. Nishida, R. Okumura, R. Sato, and K. Shirase, "Cutting Force Simulation in Minute Time Resolution for Ball End Milling Under Various Tool Posture," ASME J. of Manufacturing Science and Engineering, Vol.140, No.2, doi: 10.1115/1.4038499, 2018.
- K. Kaneko, I. Nishida, R. Sato, and K. Shirase, "Machining state monitoring in end milling based on comparison of monitored and predicted cutting torques," J. of Advanced Mechanical Design, Systems, and Manufacturing, Vol.13, No.3, doi: 10.1299/jamdsm.2019jamdsm0052, 2019.
- I. Nishida, R. Tsuyama, K. Shirase, M. Onishi, and K. Koarashi, "Development of Innovative Intelligent Machine Tool Based on CAM-CNC Integration Concept - Adaptive Control Based on Predicted Cutting Force -," Int. J. Automation Technol., Vol.13, No.3, pp. 373-381, 2019.

**Membership in Academic Societies:**  
• American Society of Mechanical Engineers (ASME)  
• Society of Manufacturing Engineers (SME)  
• Japan Society of Mechanical Engineers (JSME), Fellow  
• Japan Society for Precision Engineering (JSPE), Fellow